

# Electromagnetic Shower Properties in a Lead-Scintillator Sampling Calorimeter

Ashutosh V. Kotwal<sup>a,1</sup>, Christopher Hays<sup>b</sup>

<sup>a</sup>Physics Department, Duke University, Durham, NC 27708-0305, USA.

<sup>b</sup>Particle Physics Department, Oxford University, Keble Road, Oxford OX1 3RH, UK.

---

## Abstract

The Collider Detector at Fermilab (CDF) is a general-purpose experimental apparatus with an inner tracking detector for measuring charged particles, surrounded by a calorimeter for measurements of electromagnetic and hadronic showers. We describe a GEANT4 simulation and parameterization of the response of the CDF central electromagnetic calorimeter (CEM) to incident electrons and photons. The detector model consists of a detailed description of the CEM geometry and material in the direction of the incident particle's trajectory, and of the passive material between the tracker and the CEM. We use GEANT4 to calculate the distributions of: the energy that leaks from the back of the CEM, the energy fraction sampled by the scintillators, and the energy dependence of the response. We parameterize these distributions to accurately model electron and photon response and resolution in a custom simulation for the measurement of the  $W$  boson mass.

*Key words:* calorimeter simulation, electromagnetic shower, sampling calorimeter, energy leakage.

*PACS:* 07.05.Tp, 07.77.Ka, 07.90.+c, 29.40.-n, 29.40.Vj, 29.90.+r

---

## 1 Introduction

The measurement of the  $W$  boson mass with the CDF detector [1] at the Fermilab Tevatron  $p\bar{p}$  collider achieves a precision of 2 parts per 10,000 on the measured energy of electrons from  $W$  boson decays [2]. A key component of the energy calibration is a detailed simulation of the calorimeter response to

---

<sup>1</sup> Corresponding author. Tel: (919) 660-2563; fax: (919) 660-2525; E-mail address: ashutosh.kotwal@duke.edu

incident electrons and photons. This simulation is based on parameterizations extracted from GEANT4 [3] predictions for the distributions relevant to the measurement. In this paper we describe the GEANT4 detector model and the parameterizations of calorimeter response and resolution.

The electron energy calibration [2] is performed in two steps. First, the calibrated track momentum (with a precision of 1 part per 10,000) is transferred to the measurement of calorimeter energy, using the distribution of the ratio of calorimeter energy to the track momentum ( $E/p$ ) of electrons from the decays of  $W$  and  $Z$  bosons. In the second step, the  $Z$  boson mass ( $m_Z$ ) is measured using electrons whose cluster energy has been calibrated with  $E/p$ . After confirming the consistency of the measured  $m_Z$  with the world average [4], the  $E/p$ -based calibration is combined with the  $m_Z$ -based calibration.

There are several regimes of particle type and energy relevant to this precise calorimeter calibration: the primary electron from the  $W$  boson decay, with incident energy in the  $\approx 20$ – $60$  GeV range; radiated photons from the primary electron, with incident energies of  $\approx 1$  MeV to  $\approx 10$  GeV; and  $\approx 0.5$  –  $10$  GeV electrons from the conversion of photons<sup>2</sup> radiated by the primary electron. The CEM is a lead-scintillator sampling calorimeter. To simulate its response to incident electrons and photons of these energies, we parameterize the following quantities:

- the fraction of the incident particle’s energy that leaks out the back of the CEM;
- the fraction of the deposited energy sampled by the scintillators;
- the sampling fluctuations in the scintillator energy fraction; and
- the loss of response due to absorption and back-scatter of low-energy particles.

In the following we describe the detailed detector geometry implemented in GEANT4 (Section 2); the fractional energy leakage for a given particle type and energy (Section 3); the sampling fraction and resolution of the calorimeter (Section 4); and the absorption of energy in the passive material that results in a non-linear calorimeter response (Section 5).

## 2 Detector Model

The CDF detector [1,5,6,7] is shown in Fig. 1. The detector model implemented in the GEANT4 simulation includes the components from the outer radius of

---

<sup>2</sup> tracks with  $p_T < 500$  MeV curl up in the tracker’s magnetic field and do not reach the calorimeter.

the central tracking drift chamber [8] to the back end of the CEM calorimeter. These components are the outer aluminum casing of the tracker, the time-of-flight (TOF) system [9] attached to this casing, the solenoidal coil [10] that provides a nearly uniform 1.4 T magnetic field in the tracking volume, the central preshower system (CPR) [11] beyond the solenoid, and the CEM calorimeter (including longitudinal segmentation) [12].

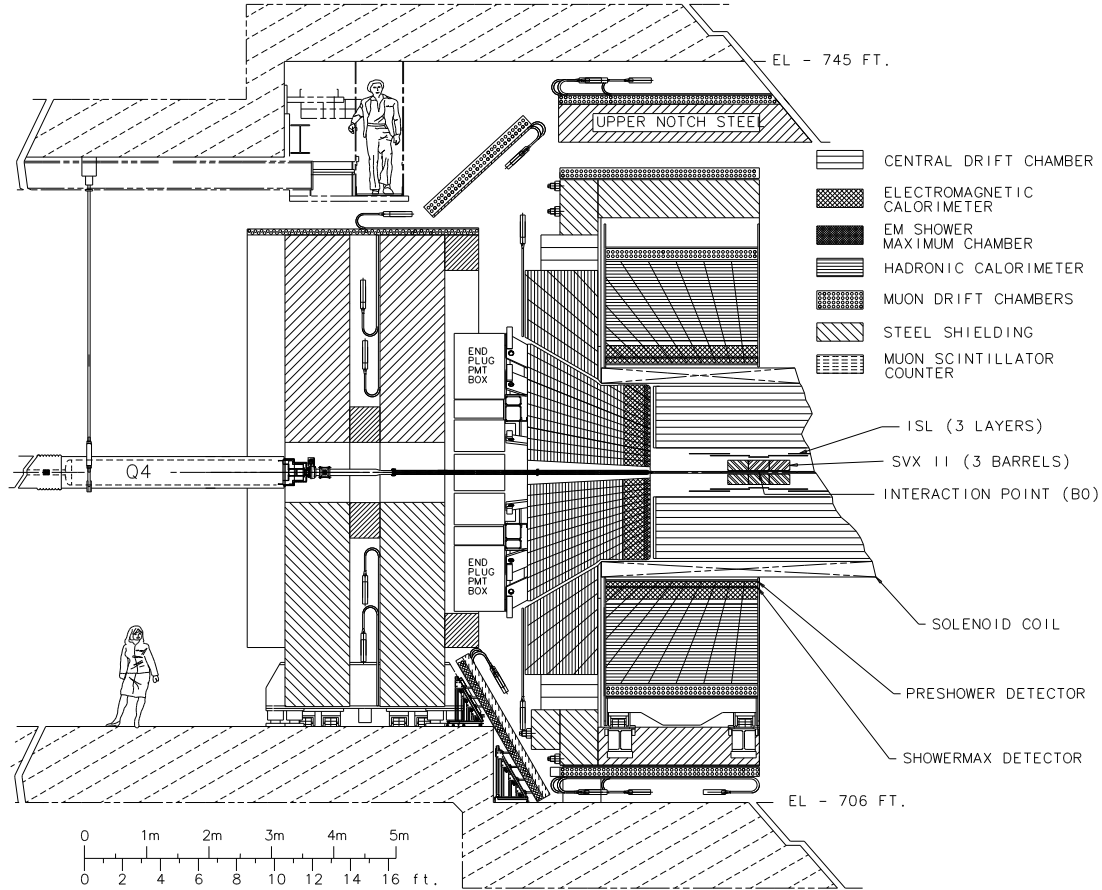


Fig. 1. A cut-away view of the CDF detector. We use a simplified GEANT4 model of the outer casing of the central drift chamber, the time-of-flight detector (not shown), the solenoid coil, the preshower detector, and the central electromagnetic calorimeter.

The CEM calorimeter is divided into  $0.1 \times 0.15 \eta - \phi$  [13] towers, shown in Fig. 2. The tower geometry depends on  $\eta$ , with towers numbered according to their distance in  $\eta$  from  $\eta = 0$ . The longitudinal segmentation of Tower 0 is an alternating system of 31 scintillator sheets and 30 aluminum-clad lead sheets, with a plate of aluminum at the front end of the tower. Each lead sheet is 3.175 mm thick and the aluminum cladding is 380  $\mu\text{m}$  thick on each side of the sheet. Each scintillator sheet is 5 mm thick. A thin (6 mm) aluminum casing contains a strip and wire chamber at the position of shower maximum (after six lead-scintillator sandwiches). Almost all the material between the tracking volume and the first scintillator – the outer casing of the tracker, the

solenoid coil and the CEM front plate – is aluminum. The TOF and CPR are a combination of scintillator and aluminum. Table 1 shows the materials in the GEANT4 model with their thicknesses in units of mm ( $x$ ) and radiation length ( $x_0 \equiv x/X_0$ ).

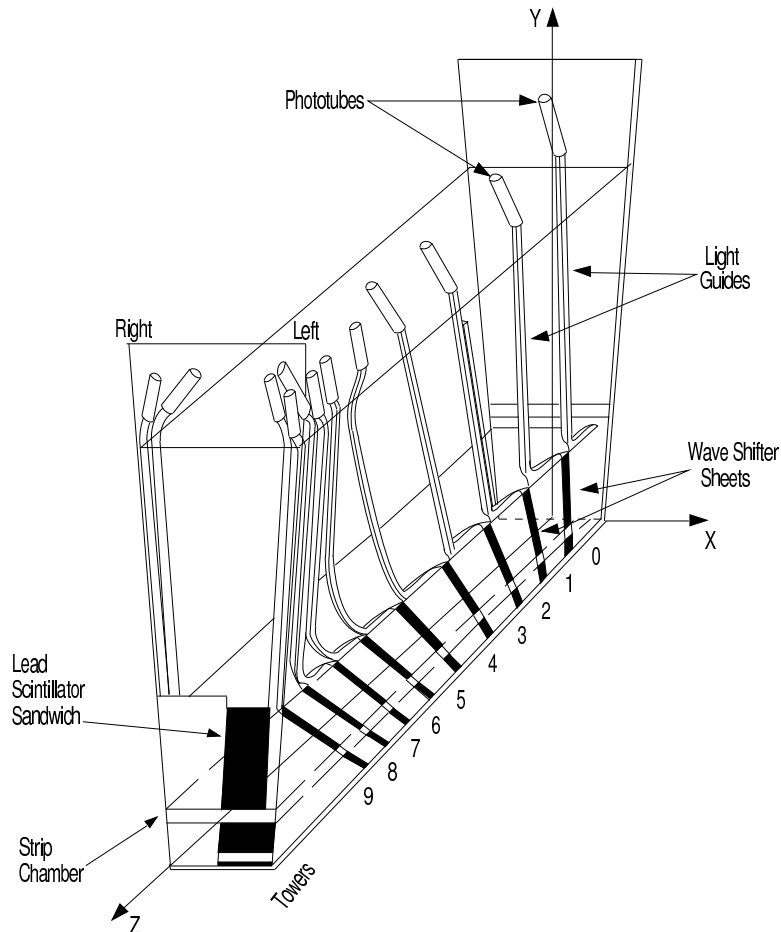


Fig. 2. The CEM calorimeter, with tower segmentation shown. The  $z$ -axis points along the beam direction towards higher pseudorapidity ( $\eta$ ), and the  $x$ -axis points in the azimuthal direction.

We model the material between the tracking volume and the first CEM scintillator as an aluminum plate of 6.51 cm thickness plus an aluminum-clad lead sheet at the front of the active calorimeter volume. The additional lead sheet is included for simplicity: with this sheet the CEM volume is modelled as 31 alternating lead-scintillator layers. Combined, the 6.51 cm of aluminum and the single lead sheet reproduce the total radiation lengths upstream of the first scintillator layer.

The geometry of other towers is implemented according to Table 2. As  $|\eta|$  increases, the number of lead sheets in a tower decreases, compensating for the increasing path length. This approximately maintains the same total number of radiation lengths traversed by a particle originating from the center of

Material	Thickness $x$ (mm)	$x_0$
CEM lead sheet	$3.175 \times 30$	$0.5658 \times 30 = 16.974$
CEM aluminum cladding	$0.76 \times 30$	$0.0085 \times 30 = 0.255$
CEM scintillator sheet	$5.0 \times 31$	$0.0121 \times 31 = 0.375$
CES aluminum	6.0	0.07
Solenoid coil aluminum	76.5	0.86
CEM front-plate aluminum	14.0	0.157
Tracker+TOF+CPR aluminum	27.0	0.303

Table 1

The materials and their thicknesses in the GEANT4 implementation of the CEM and upstream materials [12].

the detector. For each removed lead sheet, acrylic is used in its place and the subsequent scintillator sheet is blackened so that the sampling fraction is unaffected. In the GEANT4 model described here we neglect the additional radiation lengths contributed by acrylic and blackened scintillator. In the CDF measurement of the  $W$  boson mass [2] a correction is applied to account for this extra plastic material.

Tower	Thickness ( $x_0$ )	Number of lead sheets
0	17.9	30
1	18.2	30
2	18.2	29
3	17.8	27
4	18.0	26
5	17.7	24
6	18.1	23
7	17.7	21
8	18.0	20

Table 2

The thicknesses of the CEM towers [12], in units of radiation length. The aluminum front-plate is included in this calculation, but the other upstream material is not.

### 3 Longitudinal Leakage

The entire assembly of the lead-scintillator sandwich plus upstream material is about 18 radiation lengths thick. A typical 50 GeV incident electron will

deposit about 48 GeV of its energy in this structure, and about 5% will leak out the back. The leakage energy fluctuates from shower to shower, contributing to the measurement resolution of the electron’s energy. Because this resolution is not gaussian, it is important to model the leakage distribution directly. We develop parameterizations of the energy loss distributions of incident electrons and photons as functions of incident energy and angle, and of calorimeter thickness.

### 3.1 Electron Leakage Model

We define the leakage fraction  $f_l$  as the ratio of longitudinal leakage energy to the incident energy of the electron, where the incident energy is defined as the energy of the electron as it enters the outer casing of the drift chamber. Figure 3 shows the leakage fraction for three incident energies (25, 50, and 100 GeV) and for three CEM thicknesses (with 29, 30, and 31 lead-scintillator layers) for 50 GeV electrons. The distributions are skewed due to a tail that extends beyond 10%. Because of this skew it is more convenient to study the logarithm of the leakage fraction. Figure 4 shows this distribution for the same incident energies and thicknesses as Fig. 3. We find that  $\log_{10} f_l$  has a nearly invariant shape, with the peak position shifting as a function of incident energy and CEM thickness. We use this feature to devise a compact parameterization of the leakage fraction.

As shown in Fig. 5 for electrons with 50 GeV of energy normally incident on Tower 0, the standard Gamma distribution  $\Gamma(x) = x^a e^{-x}$  gives a good description of the distribution of  $\log_{10} f_l$ , with  $x \equiv (\log_{10} f_l - \mu)/\sigma$ . At this energy, the parameters of the Gamma distribution are  $a = 5$ ,  $\sigma = 0.07$  and  $\mu = -1.8$ . Of these parameters, only  $\mu = \langle \log_{10} f_l \rangle$  depends on the incident electron energy  $E$  and CEM thickness  $x_0$  at sufficiently large energy. The following parameterization accurately models this dependence for  $E > 10$  GeV:

$$\Delta\mu = (\Delta \log_2 E - \Delta x_0)/8, \tag{1}$$

implying that a change in the incident energy by a factor of two has the same effect on the leakage energy distribution as a change in the calorimeter thickness by one radiation length.

Figures 6 and 7 show the parameterization overlaid with the GEANT4 simulation for electrons with energies ranging from 1 to 25 GeV. The figures show that the parameterization breaks down for electrons with  $E < 10$  GeV. To correct this deficiency, we smear the  $\log_{10} f_l$  value drawn from the Gamma distribution by adding a random gaussian variable with mean  $0.02z$  and reso-

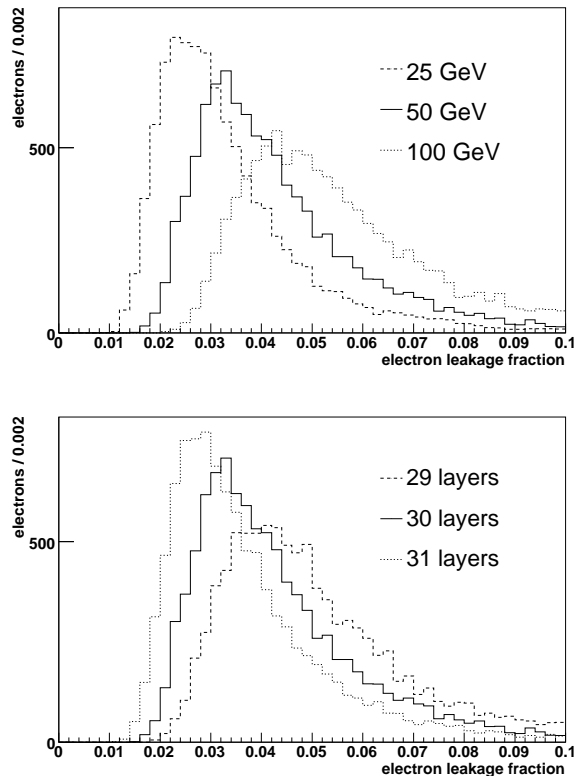


Fig. 3. Longitudinal energy leakage fraction  $f_l$  for electrons of different beam energies (top), and for CEM thicknesses varying by  $\pm 1$  lead/scintillator layer (bottom). These distributions have been calculated using our GEANT4 model.

lution  $|0.17z|$ , where  $z \equiv \log_{10}(E/50 \text{ GeV})$ . This smearing has a progressively larger effect on the distribution of  $\log_{10} f_l$  at smaller values of  $E$ . The combination of the Gamma distribution with this ad-hoc smearing models the GEANT4 distributions well. Figures 8 to 9 show the complete parameterized model compared to the GEANT4 distributions.

### 3.2 Photon Leakage Model

For high energy photons the dominant interaction mechanism is electron-positron pair production. We model the photon shower as a photon conversion followed by the showering of the resulting electron and positron. To implement this model, we generate a random variable  $d$  (in units of radiation lengths) representing the photon penetration depth before conversion. The distribution of  $d$  is given by the exponential distribution [4],

$$P(d) \propto e^{-9d/7}. \quad (2)$$

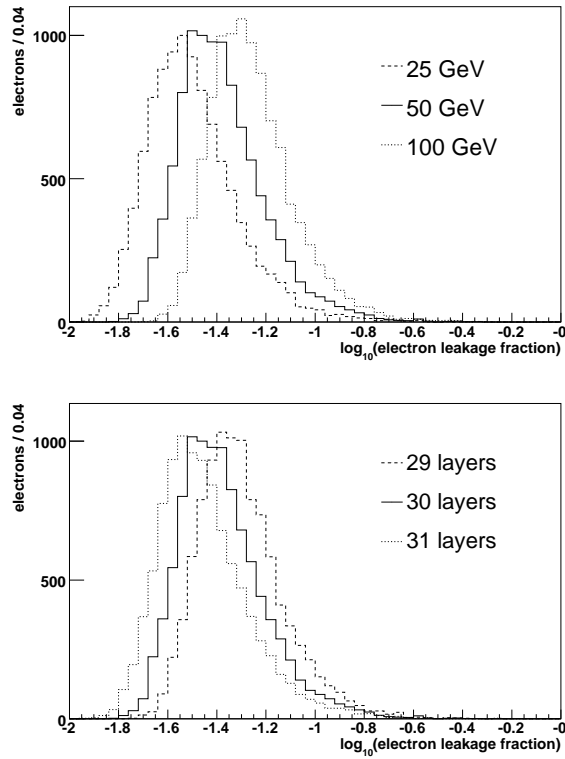


Fig. 4. The logarithm of the longitudinal energy leakage fraction  $f_l$  for incident electrons with energies of 25, 50 and 100 GeV (top), and for CEM thicknesses decreased and increased by one lead-scintillator layer (bottom) with respect to the nominal value of 30 lead sheets in Tower 0. These distributions have been calculated using our GEANT4 model.

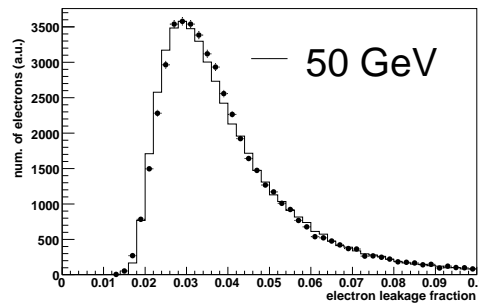


Fig. 5. A comparison of the GEANT4 model calculation (points) and our parameterization (histogram) of the distribution of the energy leakage fraction  $f_l$  for 50 GeV electrons.

Subtracting this value of  $d$  from the total thickness of the CEM in radiation lengths gives the remaining thickness through which the electron and positron propagate. The energy of the conversion electron is obtained from the spec-

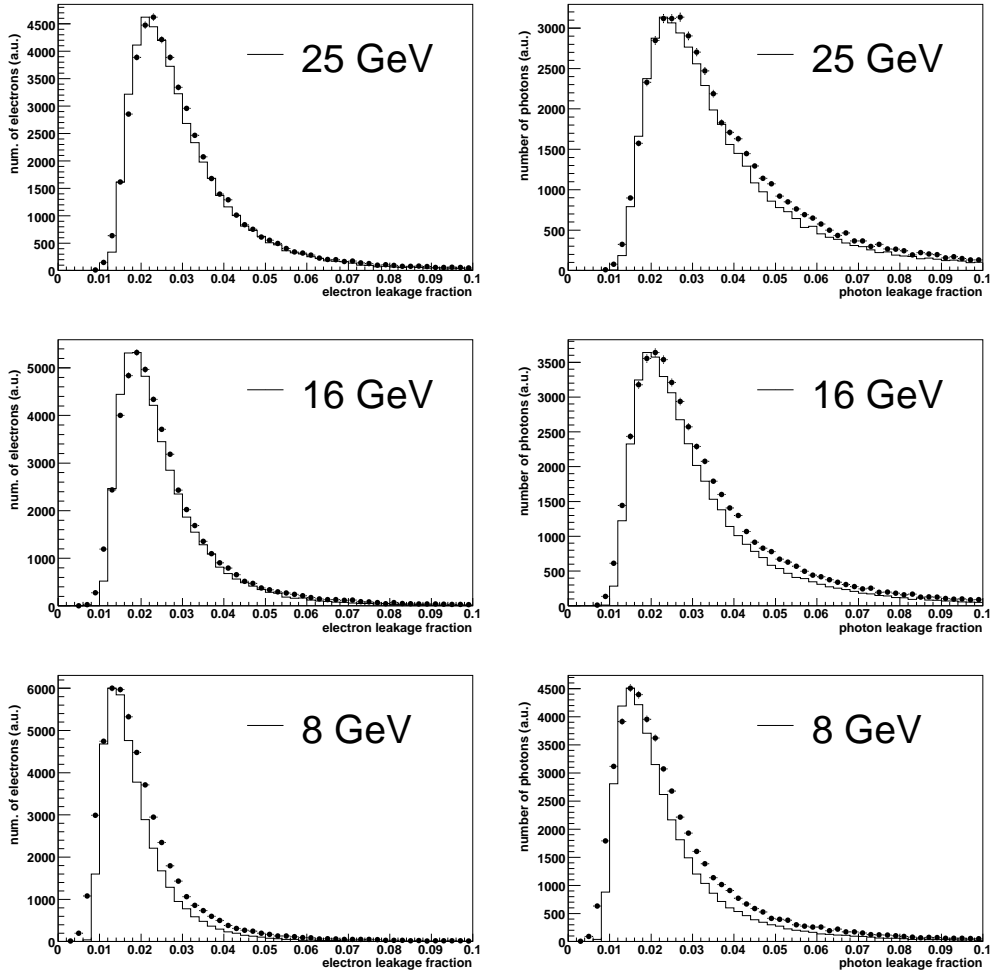


Fig. 6. Comparisons of the electron (left) and photon (right) energy leakage fraction  $f_l$  for incident energies of 25 GeV (top) to 8 GeV (bottom), showing the GEANT4 calculation (points) and our parameterization (histogram) from Eqn. 1, showing some disagreement at low energy. The final parameterization shown in Figs. 8-9 includes the ad-hoc correction to Eqn. 1 discussed in Sec. 3.1.

trum [4]

$$\frac{d\sigma}{dy} \propto 1 - 4y/3 + 4y^2/3, \quad (3)$$

where  $y$  is the fraction of the photon's energy carried by the electron. Given the electron energy and the remaining calorimeter thickness, the response for the electron and positron can be simulated using the parameterizations given earlier, yielding the effective response for the original photon. Figures 8 and 9 show that this model reproduces the GEANT4 distributions well for incident photons.

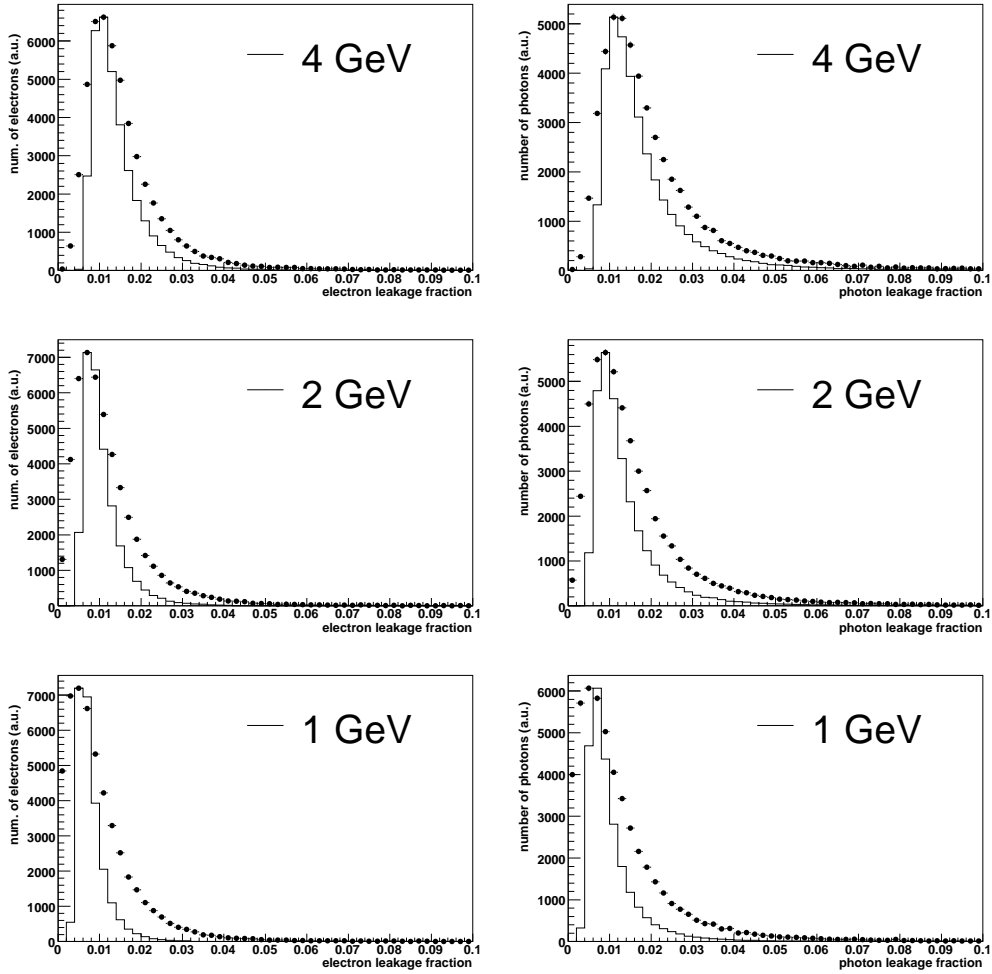


Fig. 7. Comparisons of the electron (left) and photon (right) energy leakage fraction  $f_l$  for incident energies of 4 GeV (top) to 1 GeV (bottom), showing the GEANT4 calculation (points) and the parameterization (histogram) of Eqn. 1, showing increasing disagreement at lower energy. The final parameterization shown in Figs. 8-9 includes the ad-hoc correction to Eqn. 1 discussed in Sec. 3.1.

## 4 Scintillator Sampling Model

To first order, the scintillation light produced by the shower is proportional to the energy deposited in the scintillator ( $E_s$ ). Defining the sampling fraction as  $f_s = E_s/[E(1 - f_l)]$ , where  $E$  is the incident energy, the leakage fluctuations cause the average  $f_s$  to depend on  $f_l$ . In addition, there are stochastic fluctuations in  $f_s$ .

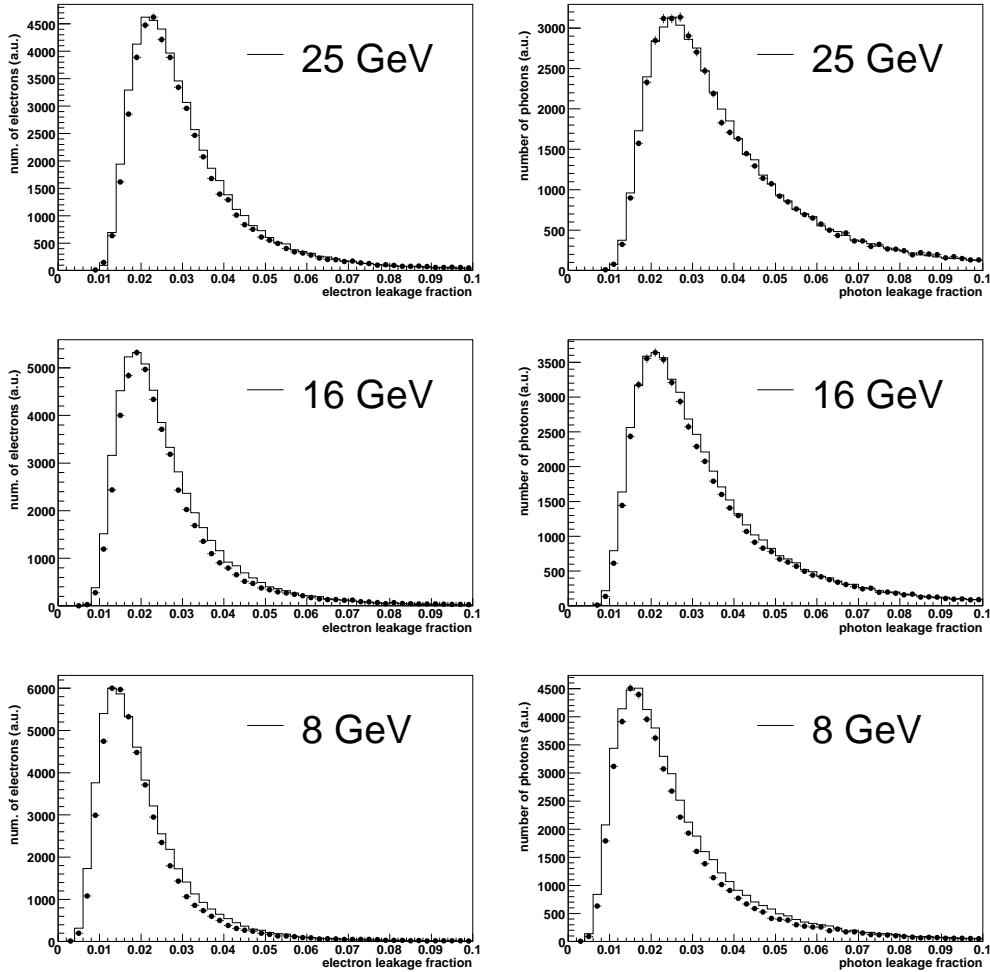


Fig. 8. Comparisons of the GEANT4 model calculation (points) and our tuned parameterization (histogram) of the distribution of the energy leakage fraction  $f_l$  for electrons (left) and photons (right) with energies ranging from of 25 GeV (top) to 8 GeV (bottom). The ad-hoc tuning improves the agreement at low energies.

#### 4.1 Leakage Dependence

We expect a positive correlation between  $f_s$  and  $f_l$  because showers that initiate early have relatively low  $f_l$  and also low  $f_s$ , since the first  $\approx 0.6$  radiation lengths are not instrumented and the scintillator layers follow the absorber in the subsequent layers. Figure 10 shows the correlation between  $f_s$  and  $f_l$  for electrons (photons) for three tower geometries: Tower 0, Tower 5 (Tower 4) and Tower 8. Since the absolute value of  $f_s$  ( $\approx 12\%$ ) is irrelevant, we rescale  $f_s$  for each plot such that  $f_s = 1$  at  $f_l = 0.01$ .

Figure 10 shows that the positive correlation between  $f_s$  and  $f_l$  grows as the tower rapidity increases. One reason for this increased correlation is the increasing amount of uninstrumented material in front of the calorimeter, due

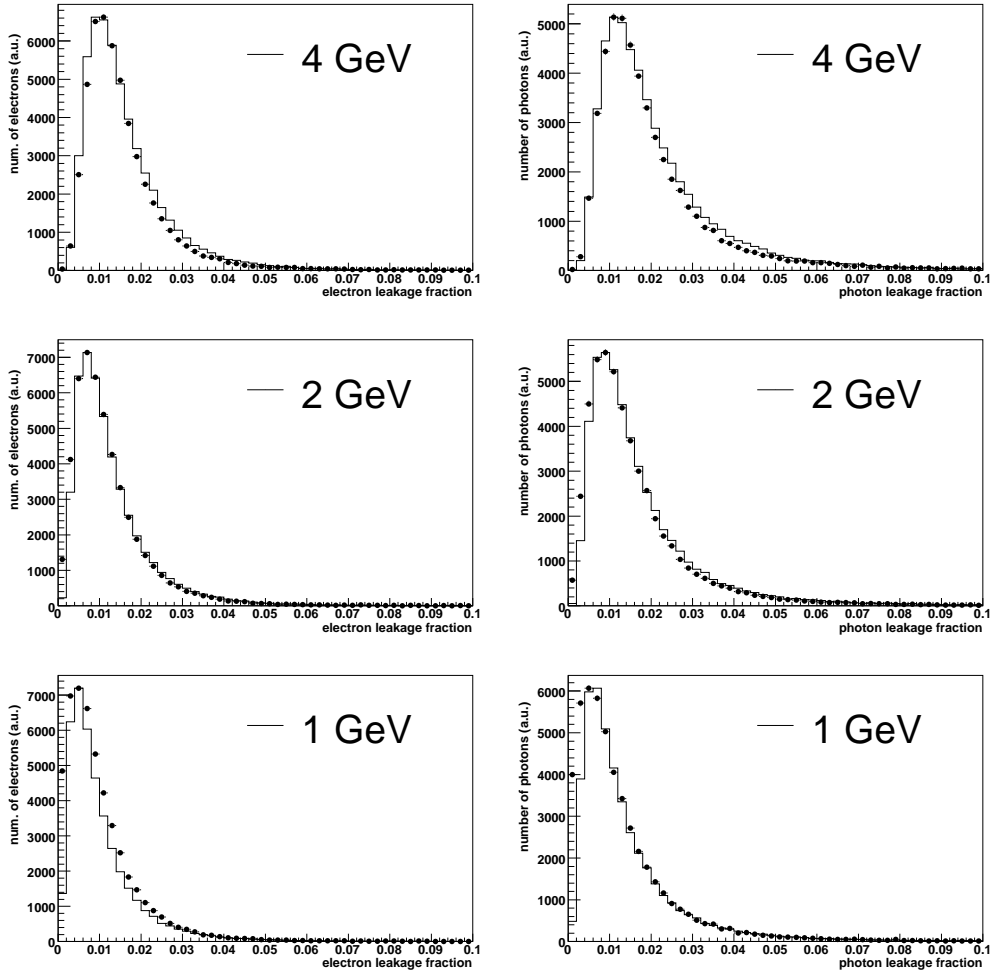


Fig. 9. Comparisons of the GEANT4 model calculation (points) and our tuned parameterization (histogram) of the distribution of the energy leakage fraction  $f_l$  for electrons (left) and photons (right) with energies ranging from of 4 GeV (top) to 1 GeV (bottom). The ad-hoc tuning improves the agreement at low energies.

to oblique incidence. Since the upstream uninstrumented material causes the positive correlation, increasing the former increases the correlation. Another reason is the reduction in the number of scintillator layers, so that each scintillator contributes a larger fraction of the total signal. Showers with higher leakage have more signal deposited in the last scintillator, giving a larger positive correlation between  $f_s$  and leakage.

The polynomial fits in Fig. 10 are used to evaluate  $\langle f_s \rangle$  for a given value of  $f_l$  in the custom simulation of electron and photon showers used for the  $W$  boson mass measurement at CDF [2].

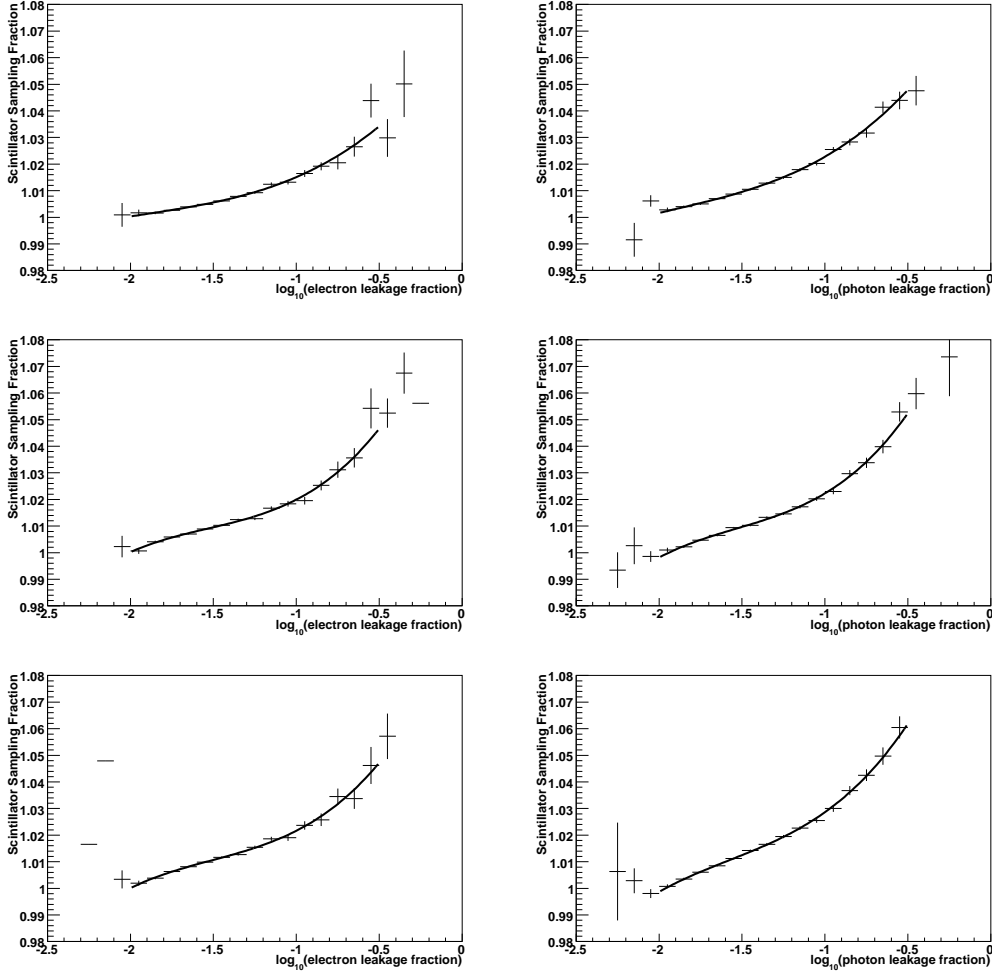


Fig. 10. The dependence of  $f_s$  on  $f_l$  for electrons (left) and photons (right) incident on Tower 0 (top), Tower 5 (middle), or Tower 8 (bottom). The curves are polynomial fits to the points calculated with the GEANT4 model. For each plot,  $f_s$  has been rescaled such that  $f_s = 1$  at  $f_l = 0.01$ .

#### 4.2 Sampling Resolution

The fluctuations in  $f_s$  correspond to the sampling resolution of the CEM, which is characterized as  $\sigma(f_s)/f_s = k/\sqrt{E_T/\text{GeV}}$ . Figure 11 shows the distributions of the normalized  $f_s$  (*i.e.*  $\langle f_s \rangle \approx 1$ ) at different energies. To remove the effect of leakage on the resolution, these distributions are obtained from GEANT4 using a very deep calorimeter with no leakage. To extract  $k$  we plot the rms of each distribution as a function of incident energy. A fit to the functional form  $k/\sqrt{E_T/\text{GeV}}$  yields  $k = 10.5\%$ . This calculation of the sampling resolution takes into account the fluctuations of the scintillator sampling fraction, but not the fluctuations of the scintillation photons and photoelectrons in the phototubes. These fluctuations contribute a sampling resolution

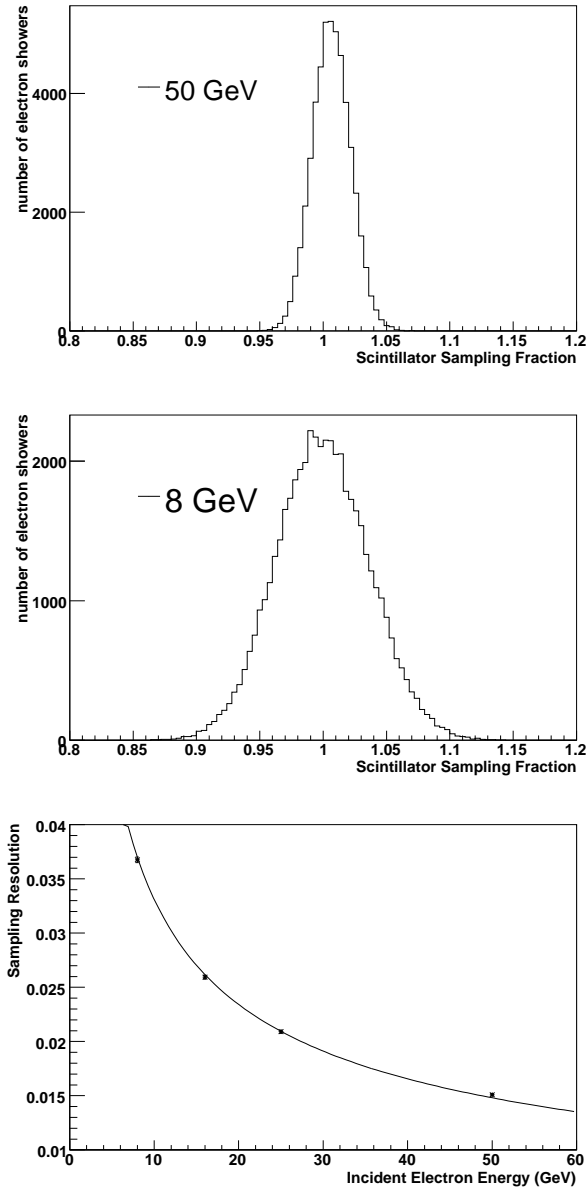


Fig. 11. Distributions of the scintillator sampling fraction  $f_s$  for electrons with incident energy of 50 GeV and 8 GeV (top and middle). The mean  $f_s$  is normalized to unity. The lower plot shows the *rms* of the  $f_s$  distribution for incident energies of 50 GeV, 25 GeV, 16 GeV and 8 GeV (points) with a fit of the form  $k/\sqrt{E/\text{GeV}}$  describing the sampling resolution.

of  $7\%/\sqrt{E_T/\text{GeV}}$  based on the measurement of 200 photoelectrons per GeV of incident energy [12]. Combining the two sources of sampling fluctuations in quadrature yields an effective sampling term of 12.6%.

## 5 Sources of Non-Linearity

A source of non-linearity at high energy is the longitudinal leakage from the back of the calorimeter, since the fraction of energy that leaks increases with energy. The parameterization of longitudinal leakage was discussed in Section 3. To isolate other sources of non-linearity, we eliminate the effect of longitudinal leakage by simulating a very deep calorimeter using GEANT4.

A deep calorimeter is expected to be linear if on average a fixed (energy-independent) fraction of the total shower energy is deposited in the scintillator layers. In the CDF detector, the uninstrumented material upstream of the CEM absorbs energy at the start of the shower without any measurement from a corresponding scintillator sampling layer. This upstream energy loss is an important source of non-linearity.

This study encompasses several additional small sources of non-linearity. First, a non-linear effect arises from the finite thickness of the lead absorber layers. In the limit of very thin absorber layers, all shower particles generated in the absorber layers traverse the entire absorber layer and deposit some fraction of their energy in the subsequent scintillator layer. In the CEM lead layers of 3.175 mm thickness, the typical ionization energy loss for an electron is 4.1 MeV per layer at normal incidence. Soft photons that convert or Compton-scatter in the front part of a lead layer can generate lower-energy electrons which are fully absorbed in the lead, leaving no signal in the subsequent scintillator. Thus, we expect a low-energy non-linearity in the calorimeter response due to the finite thickness of the lead absorber layers.

Additional non-linearities could result from the transverse leakage of the electromagnetic shower or the back-scatter of soft photons. The bulk of the unmeasured energy from these effects will be proportional to the incident energy. However, a component of this energy loss may not scale with the incoming energy, thus causing a low-energy non-linearity.

With incident electrons and photons, we use GEANT4 to calculate the energy deposited in the scintillators  $E_s$  as a function of the incident energy  $E$ . We define a low-energy non-linearity parameter  $\delta$  as

$$\delta \equiv E - \frac{E_s}{f} \tag{4}$$

where  $f$  represents a fixed scintillator sampling fraction. The quantity  $\delta$  has been defined such that  $(E - \delta)$  is strictly proportional to  $E_s$ . It represents an effective energy loss that can vary with energy, but we do not allow it to have a component proportional to energy, since this would simply redefine  $f$ .

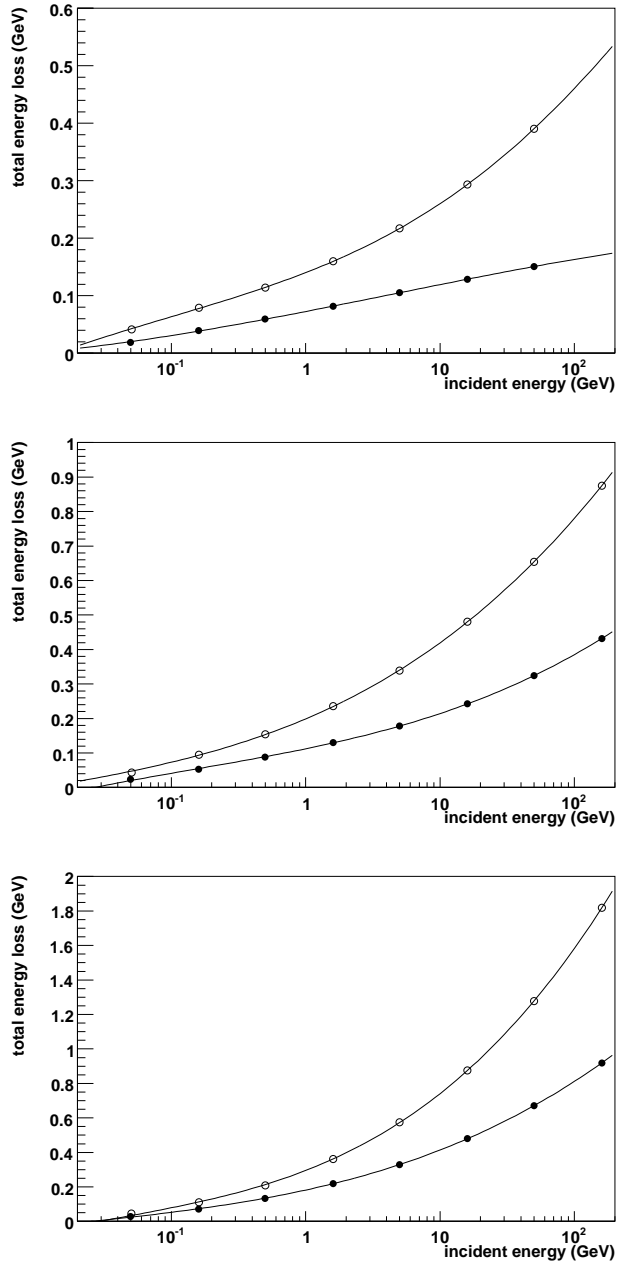


Fig. 12. The dependence of the energy loss  $\delta$  on the energy of the incident photon (open circles) and electron (solid circles), at incident angles corresponding to  $\csc \theta = 1.16$  (top),  $\csc \theta = 1.4$  (middle) and  $\csc \theta = 1.82$  (bottom). The tower geometry corresponds to a very deep calorimeter of width 48 cm. The smooth curve is a cubic polynomial fit in  $\log_{10}(E_{\text{incident}}/\text{GeV})$ .

For this study the GEANT4 detector model contains a large number of layers to fully contain the shower longitudinally. In the transverse directions we define the calorimeter to have dimensions of 48 cm  $\times$  48 cm to emulate the size of a reconstructed electron cluster used in CDF data analysis [1,7]. The GEANT4 prediction for  $\delta$  is shown in Fig. 12 for incident photons and electrons. Each

point in the figure is evaluated by averaging over 50,000 showers at fixed incident particle energies ranging from 5 MeV to 160 GeV. We see that  $\delta$  is larger for photons than electrons of the same energy, and that  $\delta$  increases logarithmically with incident energy. This increase is well-described by a function of the form

$$\delta = P_3(\log_{10} E) + \alpha E, \quad (5)$$

where  $P_3(x)$  is a cubic polynomial in  $x$ . The scintillator sampling fraction  $f$  is iteratively tuned in Eqn. 4 such that the fit returns  $\alpha = 0$ .

The non-linearity from the dominant sources – uninstrumented material upstream of the CEM and the finite thickness of the absorber sheets – tends to increase as the incidence angle of the electron or photon moves away from normal incidence. This is because the increased path length through uninstrumented material causes more early showering and therefore more unsampled energy loss. To demonstrate this dependence on incidence angle, Fig. 12 shows  $\delta$  as a function of energy for  $\csc \theta$  ranging from 1.16 to 1.82, where  $\theta = 90^\circ$  corresponds to normal incidence. The plots show that the energy loss increases with increasing  $\csc \theta$ .

## 6 Summary

We have implemented in GEANT4 the longitudinal structure of the central electromagnetic calorimeter of the CDF detector, as well as the passive material between the outer edge of the tracker and the calorimeter. Using this simulation, we calculate the longitudinal energy leakage for incident electrons as a function of incident energy and the total thickness of the structure in radiation lengths. We parameterize this distribution and derive an additional parameterization for incident photons by converting each incident photon to an electron-positron pair. We have also studied: the correlation between the energy deposited in the scintillator and the longitudinal energy leakage; the scintillator sampling fluctuations; and the calorimeter non-linearity arising from upstream passive material and finite absorber thickness. The parameterizations are used in the measurement of the  $W$  boson mass with the CDF detector.

## Acknowledgements

We wish to thank our colleagues on the CDF experiment for providing information on the construction of the detector. We thank Ravi Shekhar for his assistance in installing the GEANT4 software. We acknowledge the support

of the U.S. Department of Energy and the Science and Technology Facilities Council of the United Kingdom.

## References

- [1] CDF Collaboration (D. Acosta *et al.*), Phys. Rev. D **77**, 112001 (2008).
- [2] CDF Collaboration (T. Aaltonen *et al.*), Phys. Rev. Lett. **108**, 151803 (2012).
- [3] S. Agostinelli *et al.*, Nucl. Instrum. Meth. **A506**, 250 (2003); J. Allison *et al.*, IEEE Trans. Nucl. Sci. **53** No. 1, 270 (2006).
- [4] J. Beringer *et al.* (Particle Data Group), Phys. Rev. D **86**, 010001 (2012).
- [5] CDF Collaboration (F. Abe *et al.*), Nucl. Instrum. Meth. **A271**, 387 (1988).
- [6] CDF Collaboration (D. Acosta *et al.*), Phys. Rev. D **71**, 032001 (2005).
- [7] CDF Collaboration (A. Abulencia *et al.*), J. Phys. G: Nucl. Part. Phys. **34**, 2457 (2007).
- [8] T. Affolder *et al.*, Nucl. Instrum. Meth. **A 526**, 249 (2004).
- [9] D. Acosta *et al.*, Nucl. Instrum. Meth. **A 518**, 605 (2004).
- [10] H. Minemura *et al.*, Nucl. Instrum. Meth. **A238**, 18 (1985).
- [11] A. Artikov *et al.*, arXiv:0706.3922 (2007).
- [12] L. Balka *et al.*, Nucl. Instrum. Meth. **A267**, 272 (1988).
- [13] Pseudorapidity is defined as  $\eta = -\ln[\tan(\theta/2)]$ , where  $\theta$  is the polar angle from the beam axis. The azimuthal angle is denoted by  $\phi$ . Energy (momentum) transverse to the beam is denoted as  $E_T$  ( $p_T$ ). We use the convention  $c = 1$  throughout this paper.